

Benefic influence of nanocarbon in the bis(aryliminoethyl)pyridylnickel chloride catalyzed ethylene polymerization

Liping Zhang,^[a,b] Erlin Yue,^[b] Boping Liu,^[c] Philippe Serp,^[a] Carl Redshaw,^{*[d]}
Wen-Hua Sun^{*[b]} and Jérôme Durand^{*[a]}

[a] Laboratoire de Chimie de Coordination UPR CNRS 8241, composante ENSIACET, Université de Toulouse, 4 allée Emile Monso - CS 44362, 31030 Toulouse Cedex 4, France.

Fax: (+) 33 534323596

E-mail: jerome.durand@ensiacet.fr

[b] Key laboratory of Engineering Plastics and Beijing National Laboratory for Molecular Science, Institute of Chemistry, Chinese Academy of Sciences, Beijing 100190, China.

Fax: (+) 86 10 62618239

E-mail: whsun@iccas.ac.cn

[c] State Key Laboratory of Chemical Engineering, East China University of Science and Technology, Shanghai 200237, China.

[d] Department of Chemistry, University of Hull, Hull HU6 7RX, United Kingdom.

Abstract

A series of 1-aryliminoethylpyridine ligands (**L1**–**L3**) was synthesized by condensation of 2-acetylpyridine with 1-aminonaphthalene, 2-aminoanthracene or 1-aminopyrene. Reaction with nickel dichloride afforded the corresponding nickel (II) chloride complexes (**Ni1**–**Ni3**). All compounds were characterized and the molecular structures of **Ni1** and **Ni3** are reported. Upon activation with methylaluminoxane (MAO), all nickel complexes exhibit high activities for ethylene polymerization, producing waxes of low molecular weight and narrow polydispersity. The presence of multi-walled carbon nanotubes (MWCNT) or few layer graphene (FLG) in the catalytic medium can lead to an increase of productivity associated to a modification of the polymer structure.

Keywords : branching polyethylene - carbon nanotubes - ethylene polymerization - graphene - 2-iminopyridylnickel complex

1. Introduction

Carbon based nanomaterials like multi-walled carbon nanotubes (MWCNT) or few layer graphene (FLG) exhibit a number of attracting features including good electronic and thermal conductivity which have led in the last few years to an important interest for their use in various fields of chemical and material sciences [1]. In spite of the growing interest these materials are attracting for their use in catalytic applications [2-5], reports concerning the immobilization of discrete single site transition metal based catalysts remain scarce [6-11]. Among them, some mention the benefic influence of these carbon nanomaterials on the performances of early transition metal based olefin polymerization catalysts [12, 13]. In particular, a combination of steric and electronic effects can result in an increased molecular weight for polyethylene produced by a MWCNT/metallocene [14] or MWCNT/Ziegler-Natta [15] catalytic systems.

Since the discovery that α -diiminonickel complexes are highly active pre-catalysts for ethylene polymerization [16], extensive studies have been conducted on such systems [17]. Significant efforts have been devoted to the design of bi-dentate [18-21] or tri-dentate [22-24] ligand sets, the nickel complexes bearing bi-dentate ligands exhibiting better performances for the production of branched polyethylene. The microstructure of the polyethylene, including the molecular weight and polydispersity, could be finely tuned by employing different substituents on the ligands. To the best of our knowledge, there is no report on how the intimate interaction of CNTs or FLG with late transition metal ethylene polymerization catalysts influence the behavior of these hybrid systems. Additionally, the material properties could also be enhanced through blending. In order to extend the properties and to create hybrids of polyethylene, the influence of aryl groups based on naphthalene, anthracene and pyrene in the 2-iminopyridylnickel complex pre-catalysts have been considered (Scheme 1) with particular focus on their slightly different interactions with multi-walled carbon nanotubes (MWCNT) and few layer graphene. Their influence was reflected by the catalytic behavior of the nickel complexes. All of them promote ethylene polymerization with high catalytic activity and additionally, a positive influence of the presence of the MWCNT or FLG was observed. Herein, the synthesis and characterization of the 2-(aryliminoethyl)pyridines and their nickel complexes are reported. The catalytic performances and reaction parameters of the nickel complex pre-catalysts during ethylene polymerization were explored and are discussed in detail together with the influence of addition of small quantities of nanocarbons to the catalytic medium and the resulting effect on the obtained polyethylenes structure.

2. Experimental

2.1 General considerations

All manipulations of air and/or moisture sensitive compounds were carried out under a nitrogen atmosphere using standard Schlenk techniques. Toluene was refluxed over sodium-benzophenone and distilled under nitrogen prior to use. 2-acetylpyridine, 1-aminonaphthalene, 2-aminoanthracene and 1-aminopyrene were purchased from Alfa Chemicals. Methylaluminoxane (MAO, 1.46 M solution in toluene) and modified methylaluminoxane (MMAO, 1.93 M in heptane, 3A) were purchased from Akzo Nobel Corp. Diethylaluminum chloride (Et_2AlCl , 0.79 M in toluene) was purchased from Acros Chemicals. High-purity ethylene was obtained from Beijing Yansan Petrochemical Co. Multi-walled carbon nanotubes MWCNT (98 % purity, 2 % iron catalyst) and few layer graphene FLG were synthesized by catalytic chemical vapor deposition according to reported procedures [25, 26]. NMR spectra for the ligands were recorded on an AV 400 MHz instrument and NMR spectra for the polymer were recorded on a Bruker DMX 300 MHz instrument at ambient temperature using TMS as an internal standard. IR spectra were recorded on a Perkin Elmer spectra one spectrometer. Molecular weights (M_w) and molecular weight distributions (M_w/M_n) of the polyethylene were determined by a PL-GPC220 at 100 °C with 1,2,4-trichlorobenzene as solvent. DSC traces and melting points of polyethylene were obtained from the second scanning run on Perkin-Elmer DSC-7 at a heating rate of 10 °C/min. Thermogravimetric analysis (TGA) in air were conducted on a Setaram apparatus using a temperature program of 30-800 °C. SEM images were obtained on a JEOL JSM 6700 Field Emission Gun scanning electron microscope. Transmission electron microscope (TEM) was obtained using JEOL JEM-1400 at 120 kV.

2.2 Synthesis and characterization

Following established synthetic procedures [18-21], the condensation reaction of 2-acetylpyridine with three different aromatic amines in toluene provided the corresponding 2-imino-pyridines (**L1–L3**), which were further reacted with 0.5 equivalent of $\text{NiCl}_2 \cdot 6\text{H}_2\text{O}$ in ethanol to afford a series of bis-ligated nickel complexes in good yield (**Ni1–Ni3**) (Scheme 1).

Synthesis of the ligands L1-L3.

2-(1-(1-naphthalenylimino)ethyl)pyridine (**L1**). A mixture of 2-acetylpyridine (2.0 mmol), 1.5 eq. 1-aminonaphthalene (3.0 mmol) and a catalytic amount of p-toluenesulfonic acid were refluxed in toluene for 15 h. After the reaction, the black solid was separated by filtration and most of the solvent was removed under reduced pressure, until a black–red oil was obtained. Pentane was then added drop-wise into the solution and the colour of the solution changed from black-red to yellow.

The yellow solution was transferred to a new flask and kept at 0 °C for 15 h. **L1** was isolated as a yellow precipitate. Yield: 51 %. ¹H NMR (400 MHz, CDCl₃, 25 °C, TMS): δ 8.74 (d, *J* = 2.0 Hz, 1H, Py H); 8.50 (d, *J* = 4.0 Hz, 1H, Py H); 8.87-7.90 (m, 2H, Py H); 7.80 (d, *J* = 4.2 Hz, 1H, Ar H); 7.65 (d, *J* = 4.2 Hz, 1H, Ar H); 7.47-7.52 (m, 3H, Ar H); 7.43 (d, *J* = 3.4 Hz, 1H, Ar H); 6.84 (d, *J* = 3.2 Hz, 1H, Ar H); 2.36 (s, 3H, CH₃). ¹³C (100 MHz, CDCl₃, 25 °C, TMS): δ 168.4, 156.6, 148.7, 136.5, 128.6, 128.0, 126.4, 126.2, 125.9, 125.5, 125.0, 123.7, 123.5, 121.6, 120.8, 119.0, 16.8. FT-IR (KBr, cm⁻¹): ν 3054, 1642 (C=N), 1585, 1573, 1507, 1466, 1390, 1363, 1300, 1263, 1226, 1104, 1089, 805, 778, 743, 619. Anal. (%) for C₁₇H₁₄N₂ (246.31): Calcd. C 82.90, H 5.73, N 11.37; Found C 82.58, H 5.85, N 11.56.

The yellow solid ligands 2-(1-(2-anthracenylimino)ethyl)pyridine (**L2**) and 2-(1-(1-pyrenylimino)ethyl)pyridine (**L3**) were prepared using a similar procedure.

L2. Yield: 67 %. ¹H NMR (400 MHz, CDCl₃, 25 °C, TMS): δ 8.77 (d, *J* = 2.4 Hz, 1H, Py H); 8.57 (d, *J* = 2.4 Hz, 1H, Py H); 8.20 (s, 1H, Ar H); 8.79-7.84 (m, 2H, Py H); 7.71 (d, *J* = 3.8 Hz, 1H, Ar H); 7.62 (t, *J* = 5.0 Hz, 1H, Ar H); 7.51 (t, *J* = 5.0 Hz, 1H, Ar H); 7.25-7.30 (m, 2H, Ar H); 7.15 (d, *J* = 4.0 Hz, 1H, Ar H); 7.05 (d, *J* = 4.0 Hz, 1H, Ar H); 6.31 (s, 1H, Ar H); 1.79 (s, 3H, CH₃). ¹³C (100 MHz, CDCl₃, 25 °C, TMS): δ 164.9, 159.8, 149.5, 148.7, 137.7, 135.9, 130.7, 128.9, 128.5, 127.8, 127.7, 126.8, 125.2, 124.0, 123.9, 123.4, 122.0, 121.9, 120.7, 119.4, 29.2. FT-IR (KBr, cm⁻¹): ν 3209, 3046, 1624 (C=N), 1584, 1562, 1463, 1430, 1406, 1257, 1140, 1106, 994, 880, 786, 745, 708. Anal. (%) for C₂₁H₁₆N₂ (296.37): Calcd. C 85.11, H 5.44, N 9.45; Found C 84.83, H 5.57, N 9.60.

L3. Yield: 40 %. ¹H NMR (400 MHz, CDCl₃, 25 °C, TMS): δ 8.77 (d, *J* = 2.4 Hz, 1H, Py H); 8.58 (d, *J* = 4.0 Hz, 1H, Ar H); 8.14-8.21 (m, 2H, Py H); 8.06-8.09 (m, 2H, Ar H); 7.99-8.03 (m, 3H, Ar H); 7.92 (t, *J* = 1.8 Hz, 1H, Ar H); 7.46-7.49 (m, 2H, Ar H); 7.41 (d, *J* = 4.0 Hz, 1H, Ar H); 2.39 (s, 3H, CH₃). ¹³C (100 MHz, CDCl₃, 25 °C, TMS): δ 168.9, 156.6, 147.3, 134.9, 126.9, 126.4, 125.4, 124.5, 124.2, 123.8, 123.3, 122.0, 121.9, 119.1, 117.3, 15.1. FT-IR (KBr, cm⁻¹): ν 3039, 2963, 1638 (C=N), 1597, 1564, 1512, 1485, 1464, 1433, 1362, 1262, 1226, 1180, 1102, 1019, 880, 857, 710, 678. Anal. (%) for C₂₃H₁₆N₂ (320.39): Calcd. C 86.22, H 5.03, N 8.74; Found 85.92, H, 5.01; N 9.07.

Synthesis of the nickel complexes Ni1-Ni3.

All the nickel complexes were prepared using a similar procedure: NiCl₂·6H₂O was reacted with two equivalents of the corresponding ligand in ethanol at room temperature for 6 h (Scheme 1). The precipitate was collected by filtration, washed several times with diethyl ether and dried under reduced pressure. The desired complexes were obtained as air-stable powders in good yield and characterized by FT-IR spectroscopy, elemental analysis and X-ray diffraction for **Ni1** and **Ni3**.

The complex **Ni1** was isolated as a light green solid. Yield: 83 %. FT-IR (KBr, cm^{-1}): ν 3047, 1633, 1598, 1573, 1509, 1442, 1391, 1372, 1319, 1265, 1165, 1022, 815, 781, 646. Anal. (%) for $\text{C}_{34}\text{H}_{28}\text{Cl}_2\text{N}_4\text{Ni}$ (622.21): Calcd. C 65.63, H 4.54, N 9.00; Found C 65.33, H 4.90, N 8.79.

Complex **Ni2** was isolated as a brown solid. Yield: 80 %. FT-IR (KBr, cm^{-1}): ν 3054, 1628, 1600, 1543, 1480, 1439, 1377, 1257, 1163, 1025, 886, 780, 752, 647. Anal. (%) for $\text{C}_{42}\text{H}_{32}\text{Cl}_2\text{N}_4\text{Ni}$ (722.33): Calcd. C 69.84, H 4.47, N 7.76; Found 69.55, H 4.29, N 8.04.

Ni3 was isolated as a yellow solid. Yield: 87 %. FT-IR (KBr, cm^{-1}): ν 3046, 1626, 1597, 1569, 1441, 1372, 1321, 1257, 1185, 1049, 1021, 849, 784. Anal. (%) for $\text{C}_{46}\text{H}_{32}\text{Cl}_2\text{N}_4\text{Ni}$ (770.37): Calcd. C 71.72, H 4.19, N 7.27; Found 71.36, H 3.92, N 7.52.

X-ray crystallographic studies.

Crystals of **Ni1** and **Ni3** were obtained by laying diethyl ether onto methanol at room temperature. With graphite-monochromated Mo $K\alpha$ radiation ($\lambda = 0.71073 \text{ \AA}$), cell parameters were obtained by global refinement of the positions of all collected reflections. Intensity was corrected for Lorentz and polarization effects and empirical absorption. The structures were solved by direct methods and refined by full-matrix least squares on F². All hydrogen atoms were placed in calculated positions. Structure solution and refinement were performed by using the SHELXL-97 package [27]. Detail of the X-ray structure determinations and refinement is provided in Table 1. CCDC 935117 and 935118 contain the supplementary crystallographic data for this paper. These data can be obtained free of charge from the Cambridge Crystallographic Data Centre via www.ccdc.cam.ac.uk/data_request/cif.

2.3 General procedure for ethylene polymerization.

A 300 mL stainless steel autoclave, equipped with a mechanical stirrer and a temperature controller was employed for the reaction. Firstly, 50 mL toluene (freshly distilled) was injected into the autoclave charged with ethylene. When the temperature stabilized at the required value, another 30 mL toluene and the co-catalyst (MAO, MMAO or Et_2AlCl) were added successively by syringe. Finally, a 20 mL solution of the catalyst in toluene was injected in the reactor. The reaction mixture was intensively stirred for the desired time under constant pressure of ethylene throughout the experiment. The reaction was quenched by the addition of acidic ethanol. The precipitated polymer was washed with ethanol several times and dried under vacuum.

2.4 General procedure for ethylene polymerization in the presence of MWCNT or FLG.

The desired amount of MWCNT or FLG was placed into the reactor and the reactor was dried under vacuum. When the temperature stabilized at the required value, a 50 mL toluene solution of the nickel catalyst (5 μmol) was added to the reactor charged with 1 atm ethylene. The solution was stirred for 10 min and the desired amount of MAO and 50 mL of toluene were injected into the reactor. The ethylene pressure was immediately increased to 10 atm. After the desired duration, the reaction was quenched by addition of acidic ethanol. The precipitated polymer was washed with ethanol several times and dried under vacuum.

Table 1. Crystal data and structure refinement for **Ni1** and **Ni3**

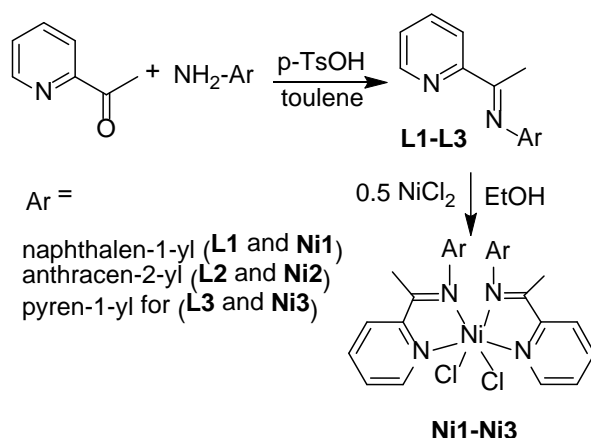
	Ni1	Ni3
empirical formula	C ₃₄ H ₂₈ Cl ₂ N ₄ Ni	C ₄₆ H ₃₂ Cl ₂ N ₄ Ni
Formula weight	622.19	770.37
<i>T</i> (K)	180(2)	110(2)
wavelength (Å)	0.71073	0.71073
cryst syst	orthorhombic	Monoclinic
space group	<i>p</i> 21 21 21	<i>C</i> 2/ <i>c</i>
<i>a</i> (Å)	8.2375(3)	29.0288
<i>b</i> (Å)	14.6511(5)	11.6481
<i>c</i> (Å)	28.2388(10)	28.0664
α (°)	90	90
β (°)	90	97.125(2)
γ (°)	90	90
<i>V</i> (Å ³)	3408.1(2)	9416.8(6)
<i>Z</i>	4	8
<i>D</i> _{calcd.} (g cm ⁻³)	1.213	1.087
μ (mm ⁻¹)	0.753	0.557
<i>F</i> (000)	1288	3184
cryst size (mm)	0.28 × 0.26 × 0.16	0.42 × 0.30 × 0.18
θ range (°)	2.57–24.27	1.41–28.15
limiting indices	–9 ≤ <i>h</i> ≤ 9	–34 ≤ <i>h</i> ≤ 38
	–16 ≤ <i>k</i> ≤ 16	–15 ≤ <i>k</i> ≤ 15
	–32 ≤ <i>l</i> ≤ 32	–37 ≤ <i>l</i> ≤ 36
no. of rflns collected	41120	47554
no. unique rflns [<i>R</i> (int)]	5520(0.0407)	11397
completeness to θ (%)	99.7%	98.6%
data/ restraints/ params	5520 / 0 / 373	11397 / 0 / 479
Goodness of fit on <i>F</i> ²	1.081	1.123
Final <i>R</i> indices [<i>I</i> > 2 σ (<i>I</i>)]	<i>R</i> 1 = 0.0344	<i>R</i> 1 = 0.0701
	w <i>R</i> 2 = 0.0882	w <i>R</i> 2 = 0.2142
<i>R</i> indices (all data)	<i>R</i> 1 = 0.0370	<i>R</i> 1 = 0.0877
	w <i>R</i> 2 = 0.0897	w <i>R</i> 2 = 0.2240
largest diff peak and hole (e Å ⁻³)	0.406 and –0.296	1.176 and –2.113

3. Results and Discussion

3.1 Synthesis and characterization of the ligands and their nickel complexes

The ligands (**L1–L3**) were readily synthesized by the condensation reaction of 2-acetylpyridine with aromatic amines (Scheme 1). All the ligands, obtained as yellow solids, were fully characterized by FT-IR, $^1\text{H-NMR}$ and $^{13}\text{C-NMR}$ spectroscopy.

The nickel complexes (**Ni1–Ni3**) were prepared by reacting $\text{NiCl}_2 \cdot 6\text{H}_2\text{O}$ with two equivalents of the corresponding ligand in ethanol at room temperature for 6 h (Scheme 1). All complexes (**Ni1–Ni3**) were isolated as air-stable powders in high yield (> 80%). By comparison with the IR spectra of the free ligands, the $\nu \text{C=N}$ stretching vibrations in complexes **Ni1–Ni3** are shifted to lower frequencies (around $1598\text{--}1600 \text{ cm}^{-1}$), indicative of an effective coordination interaction between the imino nitrogen atom and the nickel centre. The molecular structures of the complexes **Ni1** and **Ni3** were further confirmed by single-crystal X-ray diffraction studies.



Scheme 1. Synthetic procedure for nickel complexes **Ni1–Ni3**.

Crystals of complexes **Ni1** and **Ni3** suitable for single crystal X-ray analysis were grown by laying diethyl ether onto their methanol solutions at room temperature. As revealed by the molecular structure of **Ni1** (Figure 1), the nickel centre is surrounded by two bi-dentate ligands and two chlorides to afford a distorted octahedral geometry around the metal. The nickel atom deviates by 0.0182 \AA from the equatorial plane which contains N2, N4, Cl1 and Cl2. This equatorial plane and the plane formed by N1, N3 and Ni1 are almost perpendicular with a dihedral angle of 95.9° . The dihedral angle comprising the pyridine ring of one ligand and the amino-naphthalene ring of another ligand is 24.9° . However, the dihedral angle comprising of the pyridine ring of the ligand and the amino-naphthalene ring belonging to the same ligand is 77.9° . Additionally, the distance between the

pyridine ring of one ligand and the amino-naphthalene ring of the other ligand is 3.5972 Å, indicating the effective π - π interactions induced by the naphthalene ring. Considering the bond lengths around the nickel centre, the Ni1–Cl2 (2.3724(9) Å) is shorter than the bond of Ni1–Cl1 (2.4356(9) Å), whilst the bond length of Ni1–N1 (amino) is 2.067(2) Å and Ni–N2 (pyridine) is 2.135(2) Å.

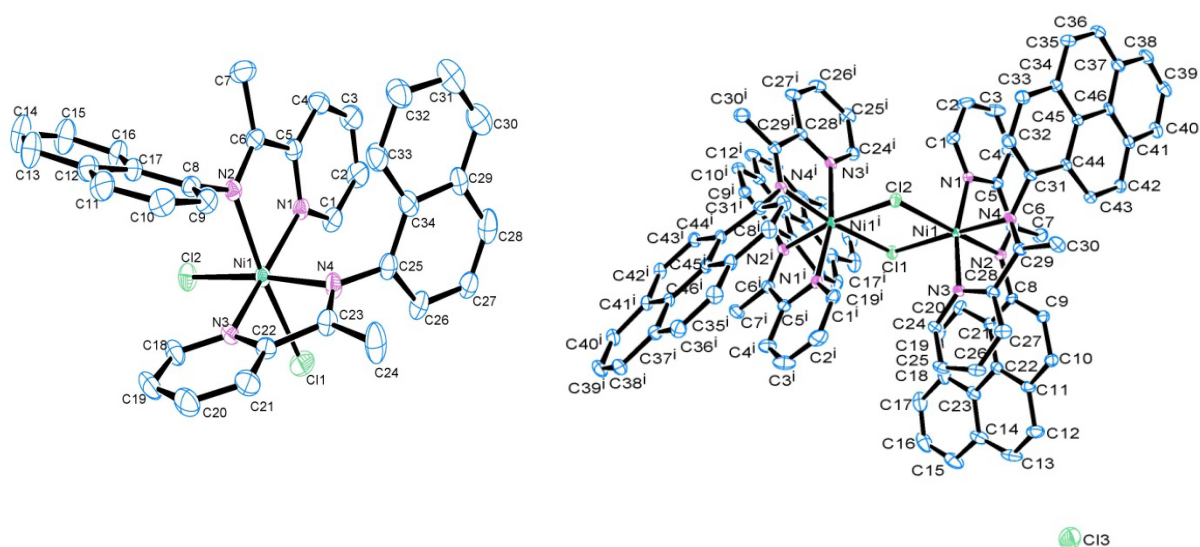


Figure 1. ORTEP molecular structure of **Ni1** (left) and **Ni3** (right). Thermal ellipsoids are shown at 30 % probability. Hydrogen atoms and solvent molecules have been omitted for clarity. Selected bond lengths (Å) and angles (°) for **Ni1**: Ni1–N1 = 2.067(2); Ni1–N2 = 2.135(3); Ni1–N3 = 2.065(2); Ni1–N4 = 2.129(3); Ni1–Cl1 = 2.4356(9); Ni1–Cl2 = 2.3724(9); N2–C6 = 1.293(4); N4–C23 = 1.278(4). N1–Ni1–N2 = 77.50(10); N1–Ni1–N3 = 164.09(10); N1–Ni1–N4 = 91.34(10); N2–Ni1–N3 = 91.80(10); N2–Ni1–N4 = 93.14(10); N3–Ni1–N4 = 77.37(10); N1–Ni1–Cl1 = 96.53(8); N2–Ni1–Cl1 = 173.83(7); N3–Ni1–Cl1 = 93.72(7); N4–Ni1–Cl1 = 85.40(8); N1–Ni1–Cl2 = 93.28(7); N2–Ni1–Cl2 = 90.28(7); N3–Ni1–Cl2 = 98.57(7); N4–Ni1–Cl2 = 174.76(8); Cl1–Ni1–Cl2 = 91.61(3). Selected bond lengths (Å) and angles (°) for **Ni2** : Ni1–N1 = 2.066(2); Ni1–N2 = 2.099(3); Ni1–N3 = 2.062(2); Ni1–N4 = 2.083(3); Ni1–Cl1 = 2.4093(8); Ni1–Cl2 = 2.4546(8); N2–C6 = 1.282(4); N4–C29 = 1.280(4). N1–Ni1–N2 = 78.43(10); N1–Ni1–N3 = 168.06(9); N1–Ni1–N4 = 93.02(9); N2–Ni1–N3 = 94.52(9); N2–Ni1–N4 = 96.28(10); N3–Ni1–N4 = 78.05(10); N1–Ni1–Cl1 = 92.95(7); N2–Ni1–Cl1 = 88.61(7); N3–Ni1–Cl1 = 96.54(7); N4–Ni1–Cl1 = 172.94(7); N1–Ni1–Cl2 = 95.71(7); N2–Ni1–Cl2 = 171.38(7); N3–Ni1–Cl2 = 92.28(7); N4–Ni1–Cl2 = 90.29(7); Cl1–Ni1–Cl2 = 85.36(3).

The molecular structure of **Ni3** (Figure 1) comprises a dimer in which the two nickel centres are linked by two bridging chloride atoms. There is no direct bonding between two nickel atoms, for which the intra-molecular distance is 3.575 Å, which is slightly longer than that (3.475 Å) observed in

other iminopyridylnickel dimers [28]. Similar to **Ni1**, the Ni centres of **Ni3** are also bound to two bidentate ligands, with Ni-N (belonging to the pyridine ring) bond lengths similar to those of **Ni1**. However, the Ni-N (belonging to the imino group) bond lengths of the **Ni3** are quite different from **Ni1**. Ni-N2 (2.099(3) Å) and Ni-N4 (2.083(3) Å) are also shorter than for **Ni1**. Moreover, the distance between the pyridine ring of one ligand and the imino-pyrene ring of the other ligand is 3.3767 Å, showing that the π - π interactions induced by the pyrene ring in **Ni3** are stronger than that of naphthalene ring in **Ni1**. This could be considered in terms of the increased potential of the **Ni3** for effective immobilization on the MWCNT or FLG through π - π interactions.

3.2 Ethylene polymerization

Prior to the investigation of the catalytic behaviour of the nickel precatalysts in the presence of nanocarbon material, we carried out an extensive optimization of their catalytic performances for ethylene polymerization under homogeneous conditions. These reactions were conducted under a 10 atm ethylene pressure. **Ni1** was subjected to a multi-parameters study (See Supplementary Material), varying the nature of the co-catalyst, the Al/Ni molar ratio, the temperature and the reaction time. Among the several alkylaluminium reagents (Et₂AlCl, MAO and MMAO) initially tested to activate complex **Ni1** at 30 °C, MAO appeared to be the best choice in terms of activity and was the selected in the subsequent screening of the nickel complexes. The molar Al/Ni ratio was also found to play an important role on the catalytic performances. In the range from 500 to 2500 the optimum ratio for both highest catalytic activity and highest M_w values for the obtained polyethylene was found to be Al/Ni = 1500. Such observations are different from other nickel complexes derived from the 2-acetylpyridine [29, 30], for which the resultant polyethylene showed lower molecular weight but higher polydispersity on increasing the Al/Ni ratio. To investigate the influence of the Al/Ni ratio on the degree of branching in the polymer, some representative polyethylene were subjected to ¹³C NMR spectroscopic analysis (Figure 2) [31] revealing a similar degree of branching at different Al/Ni ratios. The catalytic systems were then investigated over different reaction temperatures. Similar to other iminopyridine catalytic systems [23, 32, 33], the activity for polymerization decreased sharply when the reaction temperature increased from 30 °C to 50 °C, partly due to the instability of the active species at higher temperatures. However, the degree of branching in the polyethylene (PE) waxes produced at 40 °C increased sharply due to favoured chain isomerization [34, 35]. Concerning the life-time of **Ni1**, it was found that the activity decreased on increasing the reaction time (Table 2, Entries 1-4). In addition, the M_w and M_w/M_n values of the polyethylene waxes showed only a slight variation on extending the reaction time, whilst the narrow molecular distributions (1.28–1.94) were indicative of single-site active species. Examination of

the ^{13}C NMR spectra indicated that the branch number slightly decreased on increasing the reaction time.

The polymerization behaviour of **Ni2** and **Ni3** were also investigated using MAO as co-catalyst. The optimum Al/Ni ratios for **Ni2** and **Ni3** were the same as for **Ni1**. Typically, higher temperatures also proved to be detrimental to the polymerization activity. Considering the molecular weight and molecular weight distributions, the catalytic system employing **Ni2** was similar to that of **Ni1** with the range of M_w values observed from 0.6 kg mol^{-1} to 0.8 kg mol^{-1} and with M_w/M_n around 1.4. However, the M_w and M_w/M_n values of the PE waxes obtained using **Ni3** were higher than those from the other two catalytic systems (Table 2, Entries 1, 5 and 6). Whereas the catalytic activity of the **Ni3** based system is comparable to that of **Ni1**, **Ni2** proved to be significantly less productive. Therefore, only **Ni1** and **Ni3** were considered for the rest of the present study.

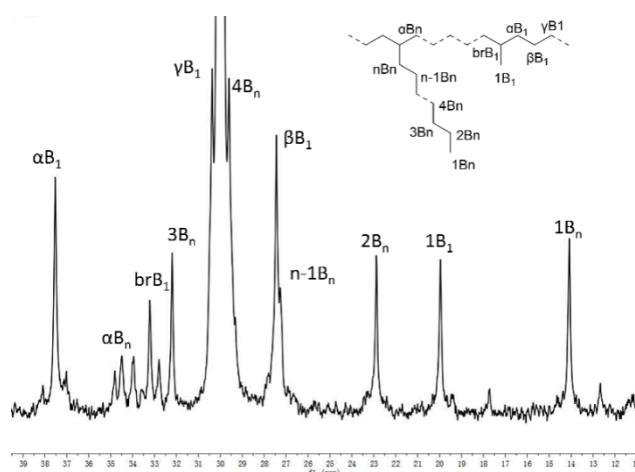


Figure 2. ^{13}C -NMR spectrum of the polyethylene prepared using the system **Ni1**/MAO.

3.3 Ethylene polymerization in the presence of MWCNT or FLG

The use of either MWCNT or FLG (Figure 3) was studied; each of them was separately added to the reaction mixture. We wanted to evaluate if their good electron conductivity will allow managing the exothermicity of the reaction, thus providing extended catalyst lifetime, and study their influence on structure of the produced polyethylene.

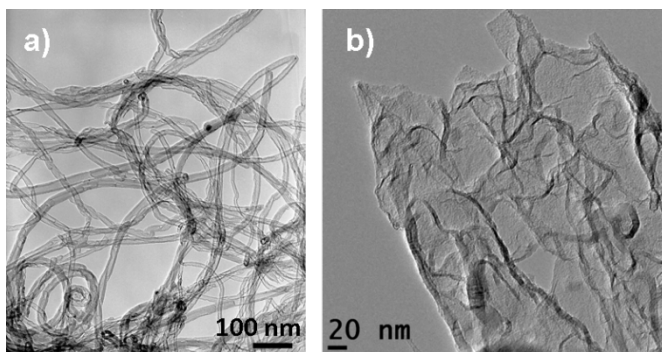


Figure 3. TEM micrographs of a) MWCNT and b) FLG used in this study.

Typically, MAO was used as the co-catalyst to generate the active nickel species. The polymerization reactions were conducted under the conditions Al/Ni = 1500, 30 °C, 30 min and 10 atm ethylene. In the presence of different amounts of MWCNT, **Ni1** and **Ni3** were studied. As shown in Table 2, the MWCNT produced a contrasted effect on the ethylene polymerization. Indeed, at low MWCNT content the activity does not change significantly, but the observed activity decreased as the amount of the MWCNT was raised (Table 2, Entries 7-10 for **Ni1** and Entries 11-13 for **Ni3**). However, PE waxes characterization by GPC and ^{13}C NMR spectroscopic analysis indicated that the PE waxes in the presence of the MWCNT were different from those produced by the nickel systems alone. For the **Ni1**/MWCNT/MAO system, unlike what reported previously for Cp_2ZrCl_2 [14] or Ziegler-Natta catalyst [15] immobilized on MWCNT, the M_w and M_w/M_n values are lower and the number of branches is higher than for the PE produced by **Ni1** in the absence of MWCNT. Similarly, when compared with **Ni3** without MWCNT, the PE waxes obtained via the **Ni3**/MWCNT/MAO system exhibited lower M_w and M_w/M_n values. In general, the catalytic activities of the nickel complex pre-catalysts decrease in the presence of MWCNT along with producing polyethylenes with lower molecular weights and narrower polydispersity suggesting that there was effective immobilization of the nickel complex on the MWCNT.

By contrast to MWCNT, the addition of FLG was positive in terms of activity for ethylene polymerization. As shown in Table 2, using **Ni1**, the best catalytic performance was observed with an amount of the graphene of 0.01 g (Table 2, Entry 15). In presence of graphene, the molecular weight of the result PE waxes were in the range of 2.40–3.53 kg mol $^{-1}$ (Table 2, Entries 14-17), which are higher than the values observed for the polymeric material produced by **Ni1** or **Ni1**/MWCNT. According to the GPC and ^{13}C NMR data for the PE waxes, higher branching was observed along with higher molecular weight distribution. Interestingly, increasing the amount of FLG (from 0.005 g to 0.04 g) led to higher molecular weight and molecular weight distribution. Such phenomenon could probably be interpreted as an increased stability of the active sites achieved using graphene.

Table 2. Ethylene polymerization with nickel pre-catalysts / MAO.^[a]

Entry	Catalyst	Nanocarbon (amount g)	t (min)	g polyethylene	Activity ^[b]	T_m (° C) ^[c]	M_w (kg.mol ⁻¹)	M_w/M_n ^[d]	Branches/ 1000C ^[e]
1	Ni1	-	30	7.78	3.11	61.07	0.90	1.74	82.0
2	Ni1	-	15	3.91	3.13	57.85	0.50	1.28	87.8
3	Ni1	-	45	10.13	2.70	60.46	0.80	1.94	76.8
4	Ni1	-	60	11.64	2.33	62.85	0.80	1.74	62.0
5	Ni2	-	30	2.29	0.92	71.71	0.70	1.37	76.5
6	Ni3	-	30	8.54	3.42	64.39	1.50	2.39	55.8
7	Ni1	MWCNT (0.005)	30	7.96	3.18	58.05	0.90	1.78	86.2
8	Ni1	MWCNT (0.01)	30	6.74	2.70	59.65	0.80	1.65	112
9	Ni1	MWCNT (0.02)	30	5.85	2.34	58.15	0.60	1.45	93
10	Ni1	MWCNT (0.04)	30	4.41	1.76	62.85	0.90	1.61	nd
11	Ni3	MWCNT (0.005)	30	8.18	3.27	67.78	0.70	1.37	nd
12	Ni3	MWCNT (0.01)	30	7.21	2.88	72.19	1.00	1.78	80.1
13	Ni3	MWCNT (0.02)	30	6.25	2.50	66.91	1.40	2.26	nd
14	Ni1	FLG (0.005)	30	9.55	3.82	51.84	3.53	6.95	163.7
15	Ni1	FLG (0.01)	30	10.6	4.22	69.31	3.00	5.41	141.1
16	Ni1	FLG (0.02)	30	8.87	3.55	53.57	2.82	5.02	nd
17	Ni1	FLG (0.04)	30	8.47	3.39	63.39	2.40	4.85	nd

[a] Reaction conditions: 5 μmol Ni; MAO : Al/Ni = 1500, 30 °C, 10 atm ethylene; 100 mL toluene.

[b] $10^6 \text{ g}\cdot\text{mol}^{-1}(\text{Ni})\cdot\text{h}^{-1}$. [c] Determined by DSC. [d] Determined by GPC. [e] Determined by ¹³C NMR.

The quality of the PE waxes made by the different kinds of pre-catalysts can be determined from TGA. The curves for the PE waxes are quite different (See Supporting Information). The decomposition temperature of the PE waxes produced by the nickel complexes is around 275 °C. The decomposition temperature of the PE waxes formed in the presence of MWCNT is around 250 °C, and the PE waxes with FLG start to decompose at 235 °C. However, if MWCNT are removed from the PE waxes/MWCNT system, the decomposition temperature of the PE waxes returns to 275 °C. This suggests that the presence of nanocarbons can lower the PE wax decomposition temperature. DSC data produced the same results. In order to characterize the PE wax coatings around the nanocarbons, SEM observations have been carried out (Figure 4). The PE wax have a regular flower-

like shape, as depicted on Figure 4-a. The aspect of the PE wax coating on MWCNT is drastically different (Figure 4-b), and it appears that the MWCNT are well dispersed into the PE waxes. Several MWCNT make bridges with the PE wax, thus acting as nodes. Since the MWCNT should interact with the nickel complex pre-catalysts, the ethylene polymerization should operate around the MWCNT, resulting in a homogeneous dispersion of MWCNT within the formed polyethylene. For the FLG/PE wax samples (Figure 4-c), it was difficult to visualize the FLG into the PE wax, but no segregation was observed, suggesting there also a homogeneous dispersion. The morphology of the polymer particles is uniform and different from the previous ones.

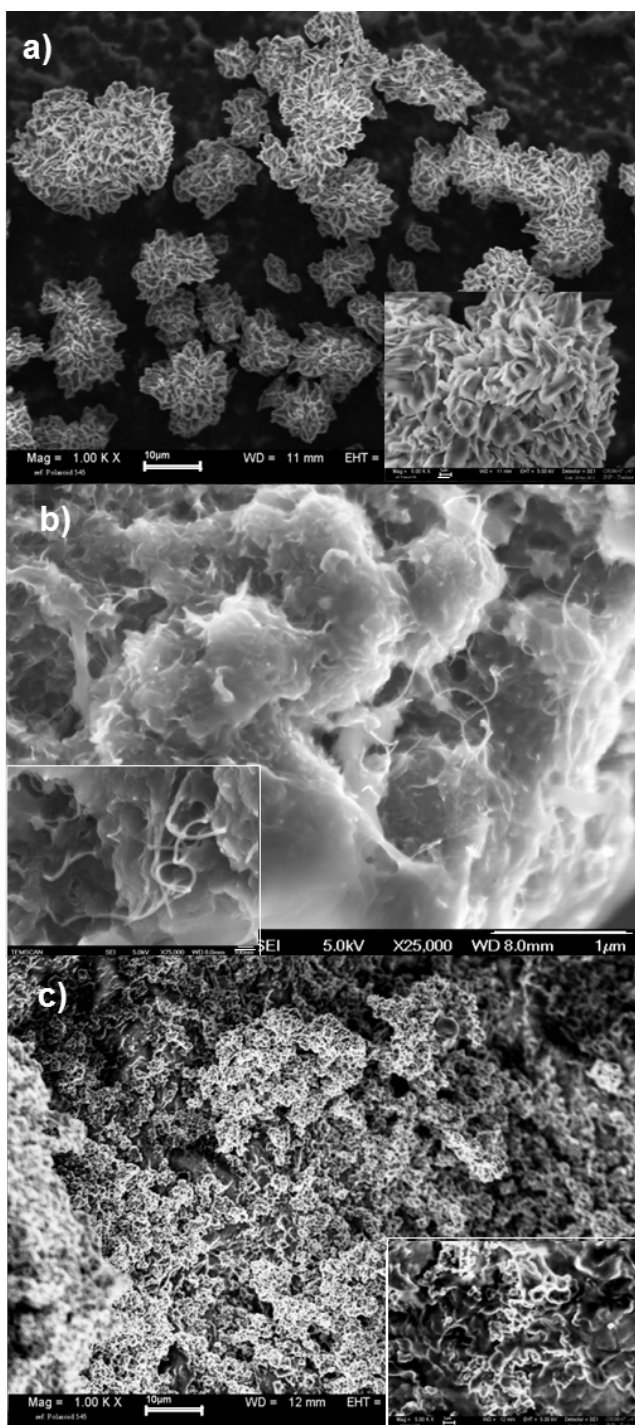


Figure 4. SEM images of a) PE wax (scale bar 10 μm, inset 1 μm); b) PE wax with MWCNT (scale bar 1 μm, inset 100 nm); and c) PE wax with FLG (scale bar 10 μm, inset 1 μm).

4. Conclusions

A series of nickel complexes bearing 1-aryliminopyridine ligands have been synthesized and fully characterized. When activated by MAO, such nickel catalysts exhibit high activities for ethylene polymerization producing polyethylene waxes of low molecular weight and narrow molecular weight distribution. In the presence of either MWCNT or FLG, the obtained polyethylenes are highly branched. The presence of MWCNT in the catalytic mixture allow the formation of polyethylene waxes of lower molecular weight and polydispersity wherer as the presence of FLG proved to be benefic for the activity of the corresponding catalytic system. The SEM observations of the PE waxes produced in the presence of nanocarbons show a homogeneous dispersion of these carbon nanomaterials in the PE matrix.

Acknowledgements

This work was supported by NSFC No. NSFC 20911130359 and ANR No. ANR-09-BLAN-0384.

The EPSRC is thanked for the award of a travel grant (to CR).

The authors are grateful to Dr. Revathi Bacsa for a gift of graphene sample.

References

- [1] M.F.L. De Volder, S.H. Tawfick, R.H. Baughman, A.J. Hart, *Science* 339 (2013) 535-539.
- [2] E. Castillejos, P.-J. Debouttière, L. Roiban, A. Solhy, V. Martinez, Y. Kihn, O. Ersen, K. Philippot, B. Chaudret, P. Serp, *Angew. Chem. Int. Ed.* 48 (2009) 2529-2533.
- [3] P. Serp, E. Castillejos, *ChemCatChem* 2 (2010) 41-47.
- [4] M. Escárcega-Bobadilla, L. Rodríguez-Pérez, E. Teuma, P. Serp, A. Masdeu-Bultó, M. Gómez, *Catal. Lett.* 141 (2011) 808-816.
- [5] A. Schaetz, M. Zeltner, W.J. Stark, *ACS Cat.* 2 (2012) 1267-1284.
- [6] W. Lu, N. Li, W. Chen, Y. Yao, *Carbon* 47 (2009) 3337-3345.
- [7] G. Liu, B. Wu, J. Zhang, X. Wang, M. Shao, J. Wang, *Inorg. Chem.* 48 (2009) 2383-2390.
- [8] P.D. Tran, A. Le Goff, J. Heidkamp, B. Jusselme, N. Guillet, S. Palacin, H. Dau, M. Fontecave, V. Artero, *Angew. Chem. Int. Ed.* 50 (2011) 1371-1374.

- [9] C. Costabile, F. Grisi, G. Siniscalchi, P. Longo, M. Sarno, D. Sannino, C. Leone, P. Ciambelli, *J. Nanosci. Nanotechnol.* 11 (2011) 10053-10062.
- [10] S. Lee, J.Y. Shin, S.-g. Lee, *Tetrahedron Lett.* 54 (2013) 684-687.
- [11] M. Blanco, P. Álvarez, C. Blanco, M.V. Jiménez, J. Fernández-Tornos, J.J. Pérez-Torrente, L.A. Oro, R. Menéndez, *ACS Cat.* 3 (2013) 1307-1317.
- [12] Y. Sánchez, C. Albano, A. Karam, R. Perera, E. Casas, *Macromol. Symp.* 282 (2009) 185-191.
- [13] D. Bonduel, M.I. Mainil, M.I. Alexandre, F. Monteverde, P. Dubois, *Chem. Commun.* (2005) 781-783.
- [14] S. Park, S.W. Yoon, K.-B. Lee, D.J. Kim, Y.H. Jung, Y. Do, H.-j. Paik, I.S. Choi, *Macromol. Rapid Commun.* 27 (2006) 47-50.
- [15] B.M. Amoli, S.A.A. Ramazani, H. Izadi, *J. Appl. Polym. Sci.* 125 (2012) E453-E461.
- [16] L.K. Johnson, C.M. Killian, M. Brookhart, *J. Am. Chem. Soc.* 117 (1995) 6414-6415.
- [17] R. Gao, W.-H. Sun, C. Redshaw, *Catal. Sci. Technol.* 3 (2013) 1172-1179.
- [18] X. Hou, Z. Cai, X. Chen, L. Wang, C. Redshaw, W.H. Sun, *Dalton Trans.* 41 (2012) 1617-1623.
- [19] H. Liu, W. Zhao, X. Hao, C. Redshaw, W. Huang, W.-H. Sun, *Organometallics* 30 (2011) 2418-2424.
- [20] J. Yu, X. Hu, Y. Zeng, L. Zhang, C. Ni, X. Hao, W.-H. Sun, *New J. Chem.* 35 (2011) 178.
- [21] L. Zhang, X. Hao, W.-H. Sun, C. Redshaw, *ACS Cat.* 1 (2011) 1213-1220.
- [22] V.C. Gibson, C. Redshaw, G.A. Solan, *Chem. Rev.* 107 (2007) 1745-1776.
- [23] X. Chen, L. Zhang, J. Yu, X. Hao, H. Liu, W.-H. Sun, *Inorg. Chim. Acta* 370 (2011) 156-163.
- [24] N. Ajellal, M.C.A. Kuhn, A.D.G. Boff, M. Hörner, C.M. Thomas, J.-F. Carpentier, O.L. Casagrande, *Organometallics* 25 (2006) 1213-1216.
- [25] R. Philippe, A. Morançais, M. Corrias, B. Caussat, Y. Kihn, P. Kalck, D. Plee, P. Gaillard, D. Bernard, P. Serp, *Chem. Vap. Deposition* 13 (2007) 447-457.
- [26] R. Bacsa, P. Serp, FR patent 11.03952 (2011).
- [27] G.M. Sheldrick, SHELXTL-97, Program for the Refinement of Crystal Structures, University of Göttingen, Germany, 1997.
- [28] T.V. Laine, M. Klinga, M. Leskelä, *Eur. J. Inorg. Chem.* (1999) 959-964.
- [29] S. Zai, H. Gao, Z. Huang, H. Hu, H. Wu, Q. Wu, *ACS Cat.* 2 (2012) 433-440.

- [30] S. Zai, F. Liu, H. Gao, C. Li, G. Zhou, S. Cheng, L. Guo, L. Zhang, F. Zhu, Q. Wu, *Chem. Commun.* 46 (2010) 4321-4323.
- [31] T. Usami, S. Takayama, *Polym. J.* 16 (1984) 731-738.
- [32] Y. Chen, P. Hao, W. Zuo, K. Gao, W.-H. Sun, *J. Organomet. Chem.* 693 (2008) 1829-1840.
- [33] P. Hao, S. Zhang, W.-H. Sun, Q. Shi, S. Adewuyi, X. Lu, P. Li, *Organometallics* 26 (2007) 2439-2446.
- [34] M.M. Wegner, A.K. Ott, B. Rieger, *Macromolecules* 43 (2010) 3624-3633.
- [35] S.D. Ittel, L.K. Johnson, M. Brookhart, *Chem. Rev.* 100 (2000) 1169-1204.